Copy 206
RM L9K10a

NACA

RESEARCH MEMORANDUM

AERODYNAMIC CHARACTERISTICS OF A WING WITH QUARTER-CHORD LINE SWEPT BACK 35°, ASPECT RATIO 6, TAPER RATIO 0.6, AND NACA 65A006 AIRFOIL SECTION

TRANSONIC-BUMP METHOD

By William C. Sleeman, Jr., and William D. Morrison, Jr.

Langley Aeronautical Laboratory
Langley Air Force Base, Va.

NATIONAL ADVISORY COMMITTEE FOR AERONAUTICS

WASHINGTON

December 12, 1949

NATIONAL ADVISORY COMMITTEE FOR AERONAUTICS

RESEARCH MEMORANDUM

AERODYNAMIC CHARACTERISTICS OF A WING WITH QUARTER-CHORD LINE SWEPT BACK 35°, ASPECT RATIO 6, TAPER RATIO 0.6, AND NACA 65A006 AIRFOIL SECTION TRANSONIC-BUMP METHOD

By William C. Sleeman, Jr., and William D. Morrison, Jr.

SUMMARY

As part of an NACA transonic research program a series of wing-body combinations are being investigated in the Langley high-speed 7- by 10-foot tunnel over a Mach number range from 0.60 to 1.18 by utilizing the transonic-bump test technique.

This paper presents the results of the investigation of a wing alone and wing-fuselage combination employing a 35° sweptback wing with aspect ratio 6, taper ratio 0.6, and an NACA 65A006 airfoil section. Lift, drag, pitching moment, and root bending moment were obtained for these configurations. In addition, effective downwash angles and dynamic-pressure characteristics in the region of a probable tail location were obtained for these configurations and are presented for a range of tail heights at one tail length. In order to expedite publishing of these data, only a brief analysis is included.

INTRODUCTION

A series of wing-body configurations are being investigated in the Langley high-speed 7- by 10-foot tunnel to study the effects of wing geometry on the longitudinal stability characteristics at transonic speeds. A Mach number range between 0.60 and 1.18 is obtained by utilizing the transonic-bump test technique.

This paper presents the results of the investigation of the wing-alone and wing-fuselage configurations employing a 35° sweptback wing with aspect ratio 6, taper ratio 0.6, and an NACA 65A006 airfoil

section. Some of the aerodynamic characteristics of a wing of aspect ratio 4, presented in reference 1, are compared with the results of the subject paper.

MODEL AND APPARATUS

The wing of the semispan model had 35° of sweepback of the quarter-chord line, taper ratio of 0.6, aspect ratio 6, and an NACA 65A006 airfoil section parallel to the free stream. The wing was made of steel and the fuselage of brass. A two-view drawing of the model is presented as figure 1, and ordinates of the fuselage of fineness ratio 10 are given in table I.

The model was mounted on an electrical strain-gage balance, which was enclosed in the bump, and the lift, drag, pitching moment, and bending moment about the model plane of symmetry were measured with calibrated galvanometers.

Effective downwash angles were determined for a range of tail heights by measuring the floating angles of five free-floating tails with the aid of calibrated slide-wire potentiometers. Details of the floating tails are shown in figures 2 and 3, and a photograph of the test setup on the bump showing three of the floating tails is given as figure 4. The tails used in this investigation were the same as those used in the investigation reported in reference 1.

A total-pressure rake was used to determine dynamic-pressure ratios for a range of tail heights along a line containing the 25-percent-mean-aerodynamic-chord points of the free-floating tails. The total-pressure tubes were spaced 0.125 inch apart for a distance of 1 inch below and 0.5 inch above the wing chord plane extended ($\alpha = 0°$) and were 0.25 inch apart for the remainder of the rake.

SYMBOLS

C_L lift coefficient (Twice panel lift/qS)

C_D drag coefficient (Twice panel drag/qS)

C_m pitching-moment coefficient referred to $0.25\bar{c}$ (Twice panel pitching moment/$qS\bar{c}$)

C_B bending-moment coefficient about root chord line (at plane of symmetry) $\left(\text{Root bending moment}/q \frac{S}{2} \frac{b}{2}\right)$

q effective dynamic pressure over span of model, pounds per square foot $\left(\frac{1}{2} \rho V^2\right)$

S twice wing area of semispan model, 0.1250 square foot

$\bar{c}$ mean aerodynamic chord of wing, 0.147 foot; based on relationship $\frac{2}{S} \int_0^{b/2} c^2 dy$ (using theoretical tip)

c local wing chord

b twice span of semispan model

y spanwise distance from plane of symmetry

ρ air density, slugs per cubic foot

V free-stream velocity, feet per second

M effective Mach number over span of model

M_l local Mach number

M_a average chordwise local Mach number

R Reynolds number of wing based on $\bar{c}$

α angle of attack, degrees

ϵ effective downwash angle, degrees

q_{wake}/q ratio of point dynamic pressure, taken along a line containing the quarter-chord points of the mean aerodynamic chords of the free-floating tails, to local free-stream dynamic pressure

y_{cp} lateral center of pressure, percent semispan $(100C_B/C_L)$

h_t tail height relative to wing chord plane extended, percent semispan, positive for tail positions above chord plane extended

TESTS

The tests were conducted in the Langley high-speed 7- by 10-foot tunnel by utilizing an adaptation of the NACA wing-flow technique for obtaining transonic speeds. The technique used involves the mounting of a model in the high-velocity flow field generated over the curved surface of a bump located on the tunnel floor (see reference 2).

Typical contours of local Mach number in the vicinity of the model location on the bump, obtained from surveys with no model in position, are shown in figure 5. It is seen that there is a Mach number variation of about 0.06 over the model semispan at low Mach numbers and from 0.08 to 0.09 at the highest Mach numbers. The chordwise Mach number generally varies less than 0.01. No attempt has been made to evaluate the effects of this chordwise and spanwise Mach number variation. Note that the long-dashed lines shown near the root of the wing (fig. 5) represent a local Mach number 5 percent below the maximum value and indicate a nominal extent of the bump boundary layer. The effective test Mach number was obtained from contour charts similar to those presented in figure 5 by using the relationship

$$M = \frac{2}{S}\int_0^{b/2} cM_a \, dy$$

The variation of mean test Reynolds number with Mach number is shown in figure 6. The boundaries in the figure indicate the range in Reynolds number caused by variations in test conditions in the course of the investigation.

Force and moment data, effective downwash angles, and the ratio of dynamic pressure at 25 percent of the tail mean aerodynamic chord to free-stream dynamic pressure were obtained for the model configurations through a Mach number range of 0.60 to 1.18 and an angle-of-attack range of -4° to 10°. Pitching-moment data were obtained about an axis passing through the 25-percent-mean-aerodynamic-chord point.

The end-plate tares on drag were obtained through the Mach number range at 0° angle of attack by testing the model configurations without end plates as shown in figure 7 for the wing-alone configuration. A gap of about 1/16 inch was maintained between the wing surface at the root chord and the bump surface and a sponge-wiper seal was fastened to the wing butt beneath the surface of the bump to minimize leakage. The drag end-plate tares were assumed to be constant with angle of attack and the tares obtained at zero angle of attack were applied to all drag

data. A similar end-plate correction has been applied to the downwash data. No base-pressure correction has been applied to the wing-fuselage drag data. Jet-boundary corrections have not been evaluated because the boundary conditions to be satisfied are not rigorously defined. However, inasmuch as the effective flow field is large compared to the span and chord of the model, the corrections are believed to be small.

By measuring tail floating angles without a model installed it was determined that a tail spacing of 2 inches would produce negligible interference effects of reflected shock waves on the tail floating angles. Downwash angles for the wing-alone configuration were therefore obtained simultaneously for the middle, highest, and lowest tail positions in one series of tests and similarly for the two intermediate positions in succeeding runs. (See fig. 3.) For the wing-fuselage tests the effective downwash angles at the chord plane extended were determined by mounting a free-floating tail on the center line of the fuselage. The downwash angles presented are increments from the tail floating angles without a model in position. It should be noted that the floating angles measured are in reality a measure of the angle of zero pitching moment about the tail pivot axis rather than the angle of zero lift. It has been estimated, however, that for the tail arrangement used a downwash gradient of 2° across the span of the tail will result in an error of less than 0.2° in the measured downwash angle.

Total-pressure readings were obtained at constant angles of attack through the Mach number range without an end plate on the model and with the gap between the bump cutout and wing butt sealed with a sponge seal to eliminate end-plate wake and minimize leakage effects. The static-pressure values used in computing the dynamic-pressure ratios were obtained by use of a static probe with no model in position.

RESULTS AND DISCUSSION

The figures presenting the results are as follows:

The discussion is based on the summarized values given in figure 14 unless otherwise noted. The slopes summarized in figure 14 have been averaged over a range of ±0.10 of the stated lift coefficient.

Lift and Drag Characteristics

The lift-curve slope measured near zero lift for the wing alone was approximately 0.076 at a Mach number of 0.60. This value compares with a value of 0.073 estimated for this Mach number by use of the charts in reference 3. The wing-alone lift-curve slope was an average of about 12 percent higher throughout the test Mach number range than for the wing of aspect ratio 4 (reference 1) which, except for aspect ratio, had geometry similar to the present wing. The addition of the fuselage increased the lift-curve slope from 3 to 6 percent throughout the Mach number range investigated. This increase was about half the fuselage effect shown for the wing of aspect ratio 4 of reference 1.

The drag rise at zero lift began at a Mach number slightly above 0.90 for the wing alone. For the wing-fuselage configuration the drag rise was slightly earlier and steeper than for the wing alone. The drag data for the 35° sweptback wing of aspect ratio 4 issued in reference 1 are not directly comparable with the present results because the drag data of reference 1 were not corrected for end-plate tares. Subsequent to the issuance of reference 1, drag data were obtained for the wing of reference 1 by using the sponge-wiper-seal technique described in this paper. These data are presented in figure 15 together with the results from the wing of aspect ratio 6 of this paper for comparison. For both the wing-alone and wing-fuselage configurations, increasing the aspect ratio from 4 to 6 decreased the drag slightly at Mach numbers below approximately $M = 1.0$ and appeared to delay the drag rise Mach number slightly. At Mach numbers above unity the drag was higher for the wing of aspect ratio 6, especially for the wing-fuselage configuration.

The lateral center of pressure for the wing alone (at lift coefficients below 0.4) was located at 45 percent of the semispan at a Mach number of 0.60. This value compares with an estimated low-speed value of 45.7 percent (reference 3). As the Mach number increased y_{cp} moved outboard gradually to 48 percent of the semispan at $M = 0.95$ and remained constant up to the highest test Mach number. The addition of the fuselage moved y_{cp} inboard approximately 3 percent of the semispan throughout the test Mach number range.

Pitching-Moment Characteristics

At a Mach number of 0.60 the aerodynamic-center location near zero lift for the wing alone was 34 percent of the mean aerodynamic chord $\left(\left(\frac{\partial C_m}{\partial C_L}\right)_M = -0.09\right)$. The estimated low-speed aerodynamic-center location (reference 3) was 25.2 percent of the mean aerodynamic chord. In general the wing-alone aerodynamic-center locations obtained at a Mach number of 0.60 in this series of bump investigations have indicated a somewhat more rearward position of the aerodynamic center than predicted from the charts of reference 3. A forward movement of the aerodynamic center to 29 percent of the mean aerodynamic chord occurred between $M = 0.60$ and $M = 0.85$. The aerodynamic center moved rearward gradually as the Mach number increased above 0.85 and was located at 40 percent of the mean aerodynamic chord at Mach numbers above $M = 1.05$. The addition of the fuselage was destabilizing throughout the test Mach number range with a minimum forward aerodynamic-center movement at $M = 0.85$.

The wing-alone and wing-fuselage pitching-moment curves (figs. 8 and 9) indicate instability at higher lift coefficients for Mach numbers below approximately $M = 0.98$. However, above $M = 1.00$ there is no indication of this instability even at the highest lift coefficients attained. Similar trends in pitching-moment characteristics were found in the results presented in reference 1.

Downwash and Dynamic Pressure

The variation of effective downwash angle with tail height and angle of attack for the wing-alone and wing-fuselage configurations at various Mach numbers is presented in figures 10 and 11. The downwash gradient $(\partial\epsilon/\partial\alpha)_M$ near zero lift for the wing alone (fig. 12) was practically invariant with tail height throughout the Mach number range investigated. The addition of the fuselage caused an appreciable increase in $(\partial\epsilon/\partial\alpha)_M$ for tail positions near the chord plane extended. The variation of $(\partial\epsilon/\partial\alpha)_M$ with Mach number (fig. 14) for $h_t = 0$ and ± 30 indicated a decrease in downwash gradient of approximately 50 percent between $M = 0.90$ and $M = 1.15$ for both the wing-alone and wing-fuselage configurations.

The test angle-of-attack range with the free-floating tail slightly below the chord plane extended was restricted by the presence of the fuselage.

The results of the point dynamic-pressure surveys made along a line containing the 25-percent-mean-aerodynamic-chord points of the free-floating tails used in the downwash surveys are presented in

figure 13. The maximum loss in dynamic pressure at the wake center line for high angles of attack was about 17 percent for the wing alone. At a constant angle of attack the Mach number effects on the wake characteristics are small, especially at low angles of attack. The addition of the fuselage showed only a small effect on the wake profiles although the peak losses at the highest test angle of attack were slightly reduced at subsonic Mach numbers.

Langley Aeronautical Laboratory
National Advisory Committee for Aeronautics
Langley Air Force Base, Va.

REFERENCES

1. Sleeman, William C., Jr., and Becht, Robert E.: Aerodynamic Characteristics of a Wing with Quarter-Chord Line Swept Back 35°, Aspect Ratio 4, Taper Ratio 0.6, and NACA 65A006 Airfoil Section. Transonic-Bump Method. NACA RM L9B25, 1949.

2. Schneiter, Leslie E., and Ziff, Howard L.: Preliminary Investigation of Spoiler Lateral Control on a 42° Sweptback Wing at Transonic Speeds. NACA RM L7F19, 1947.

3. DeYoung, John: Theoretical Additional Span Loading Characteristics of Wings with Arbitrary Sweep, Aspect Ratio, and Taper Ratio. NACA TN 1491, 1947.

CONFIDENTIAL

TABLE I.- FUSELAGE ORDINATES

[Basic fineness ratio 12; actual fineness ratio 10 achieved by cutting off the rear one-sixth of the body; $\bar{c}/4$ located at $l/2$]

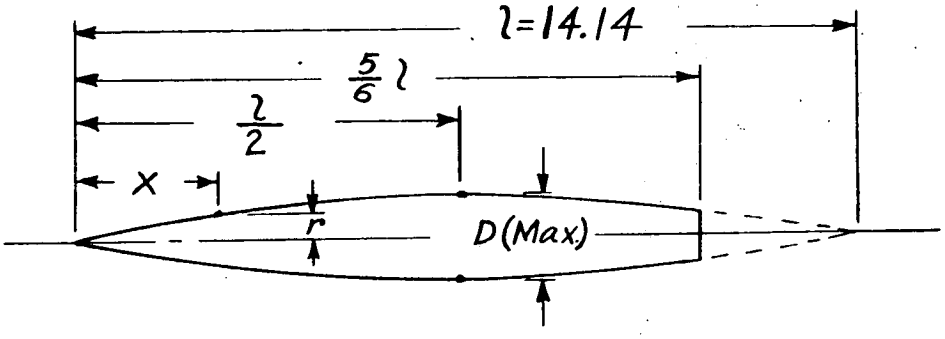

Ordinates			
x/l	r/l	x/l	r/l
0	0	0	0
.005	.00231	.4500	.04143
.0075	.00298	.5000	.04167
.0125	.00428	.5500	.04130
.0250	.00722	.6000	.04024
.0500	.01205	.6500	.03842
.0750	.01613	.7000	.03562
.1000	.01971	.7500	.03128
.1500	.02593	.8000	.02526
.2000	.03090	.8338	.02000
.2500	.03465	.8500	.01852
.3000	.03741	.9000	.01125
.3500	.03933	.9500	.00439
.4000	.04063	1.0000	0
L. E. radius = 0.00051			

CONFIDENTIAL

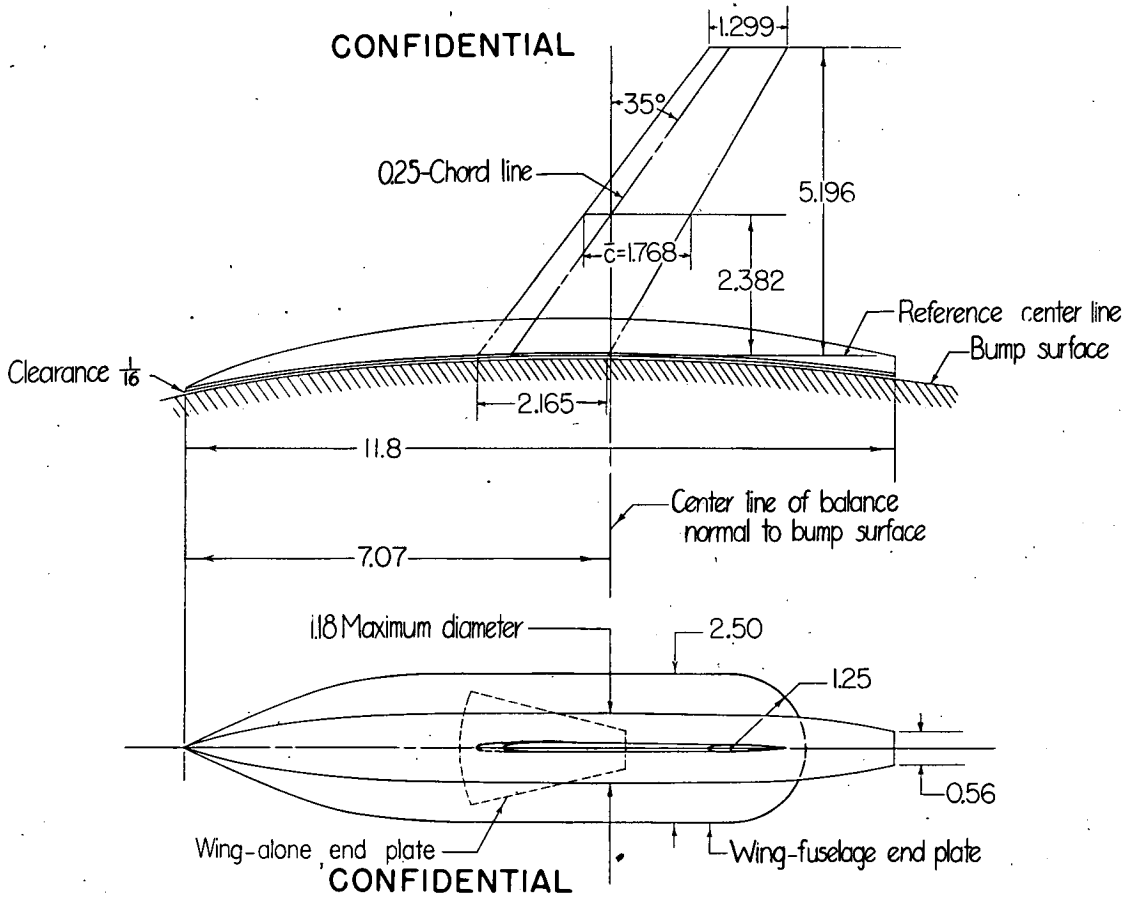

Tabulated Wing Data	
Area (Twice semispan)	0.125 sq ft
Mean aerodynamic chord	0.1473 ft
Aspect ratio	6.0
Taper ratio	0.6
Incidence	0.0°
Dihedral	0.0°
Airfoil section parallel to free stream	NACA 65A006

All dimensions in inches

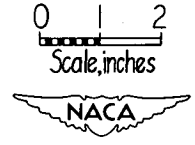

Figure 1.- General arrangement of model with 35° sweptback wing, aspect ratio 6, taper ratio 0.6, and NACA 65A006 airfoil.

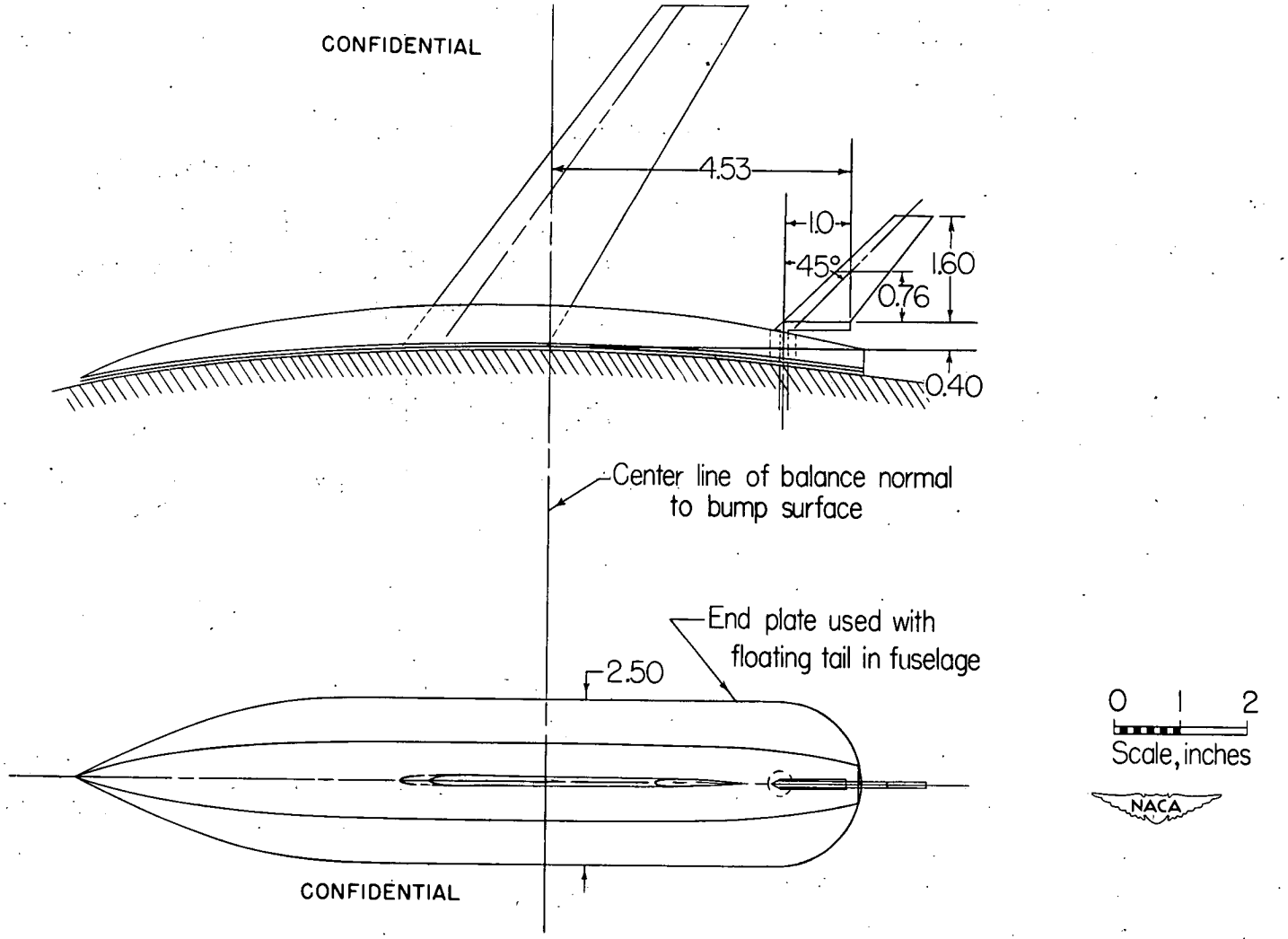

Figure 2.- Details of free-floating tail mounted in fuselage of a model with 35° sweptback wing, aspect ratio 6, taper ratio 0.6, and NACA 65A006 airfoil.

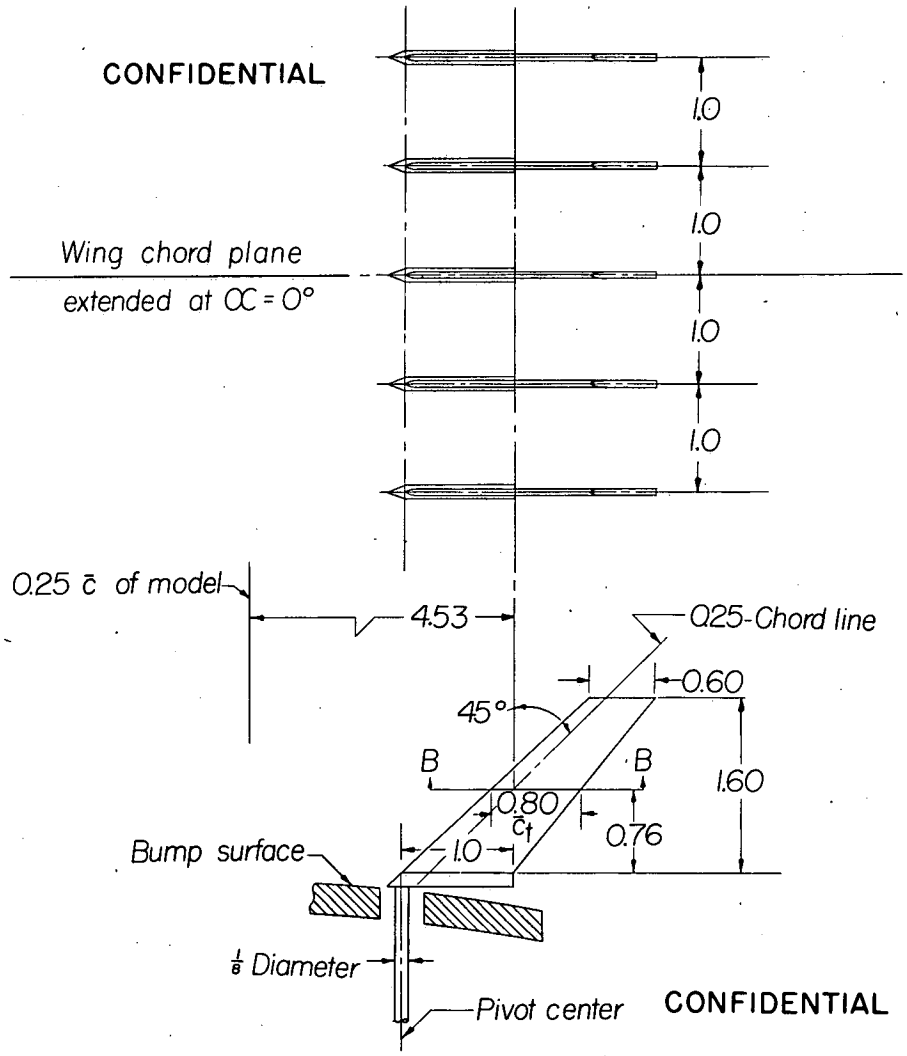

Floating-tail geometry

Area (Twice semispan)	*0.0178 sq ft*
Aspect ratio	*4.0*
Taper ratio	*0.60*

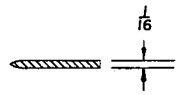

Section B-B

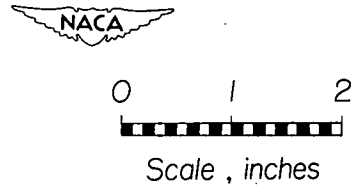

Figure 3.- Details of free-floating tails used in surveys behind model with 35° sweptback wing, aspect ratio 6, taper ratio 0.6, and NACA 65A006 airfoil.

Figure 4.- Photograph of model with 35° sweptback wing, aspect ratio 6, taper ratio 0.6, and NACA 65A006 airfoil.

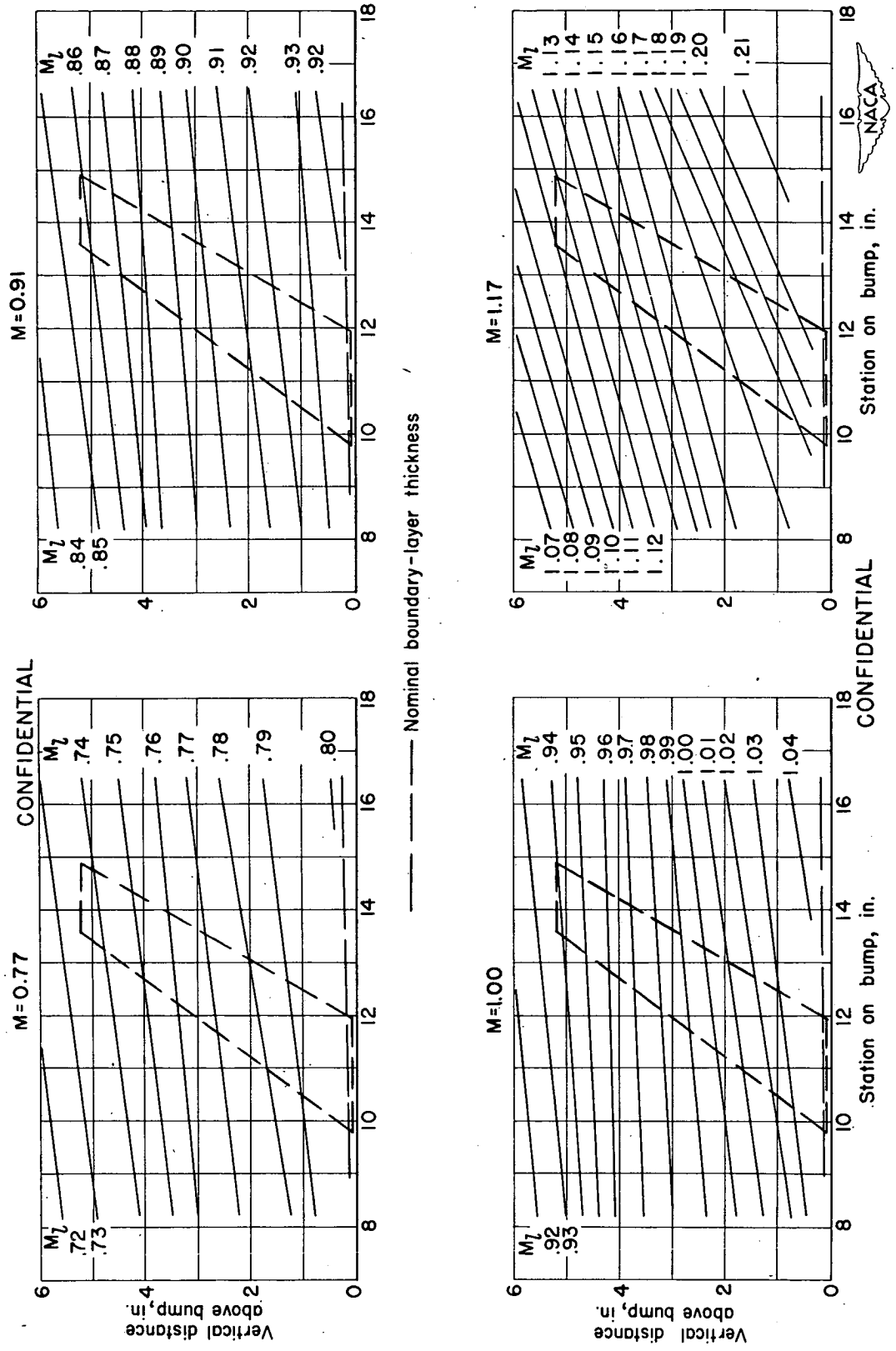

Figure 5.- Typical Mach number contours over transonic bump in region of model location.

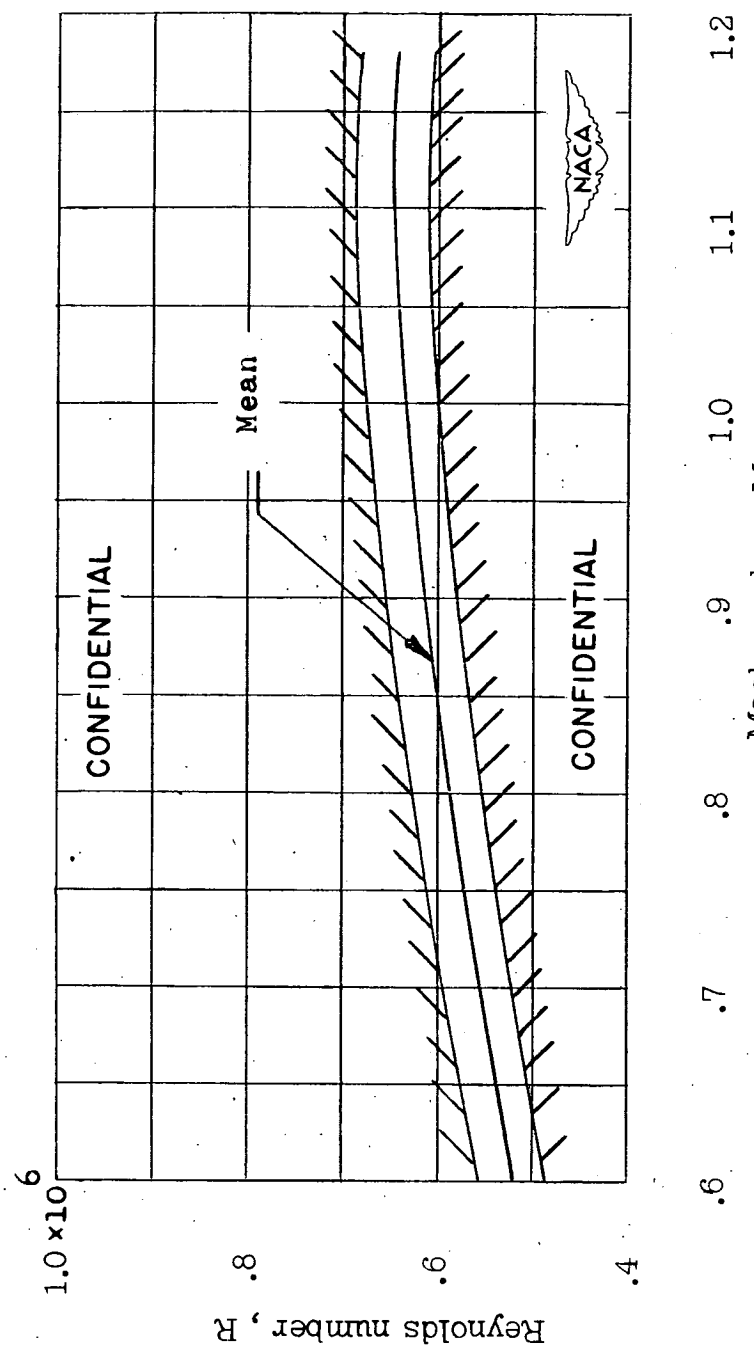

Figure 6.- Variation of test Reynolds number with Mach number for model with 35° sweptback wing, aspect ratio 6, taper ratio 0.6, and NACA 65A006 airfoil.

CONFIDENTIAL

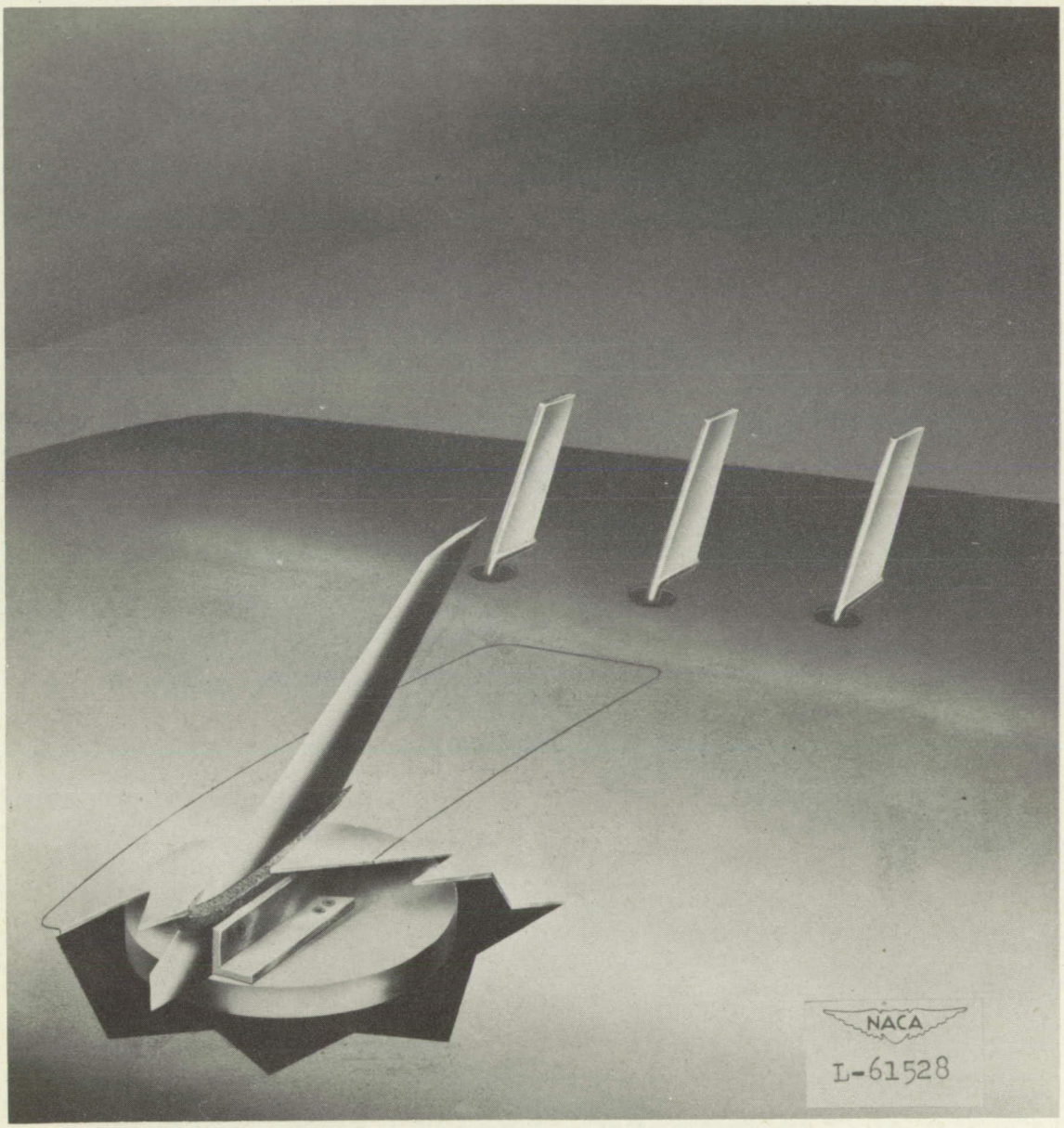

Figure 7.- A view of the model mounted on the balance showing the sponge-seal arrangement used in determining end-plate tares.

CONFIDENTIAL

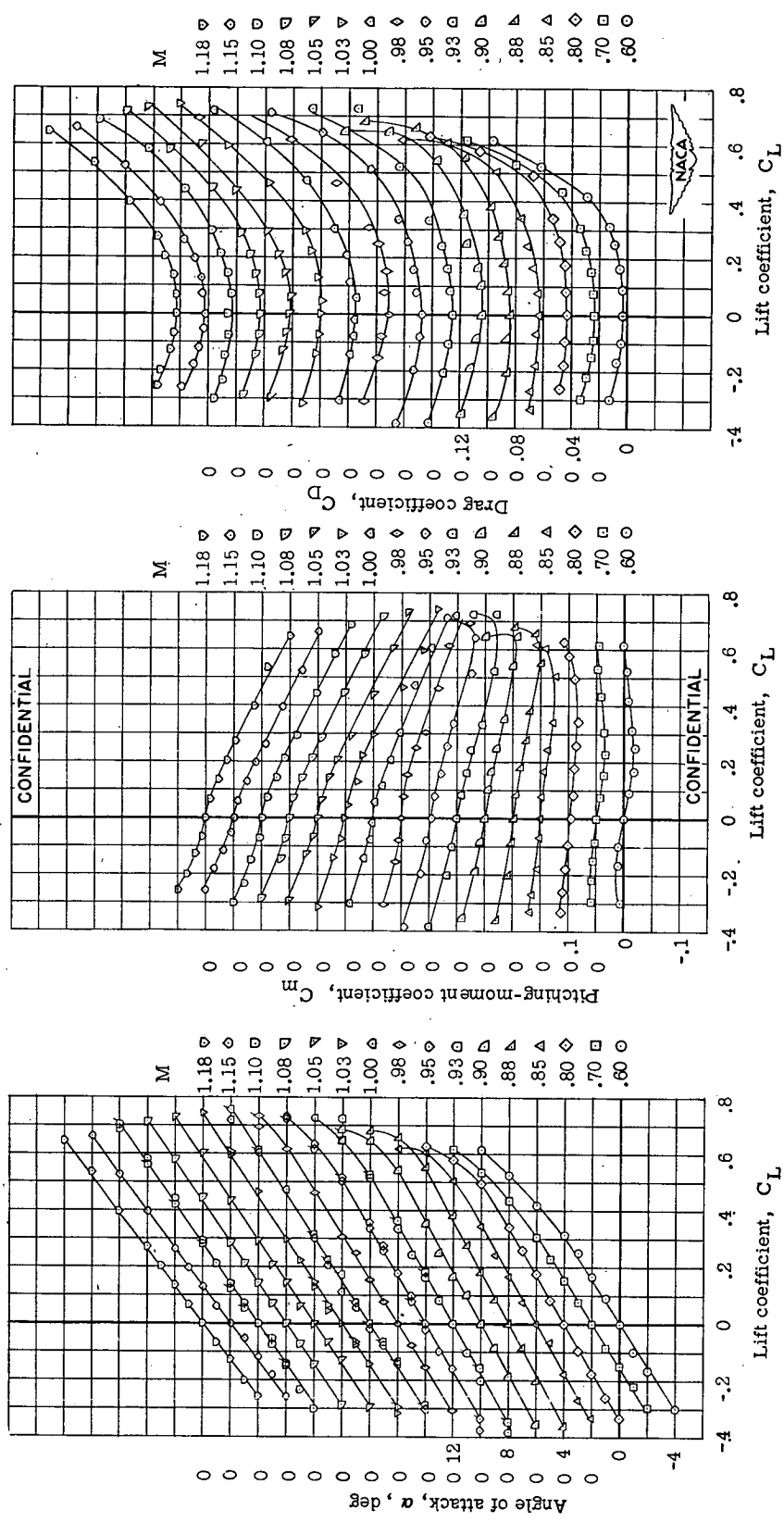

Figure 8.- Wing-alone aerodynamic characteristics for model with 35° sweptback wing, aspect ratio 6, taper ratio 0.6, and NACA 65A006 airfoil. Check points are indicated by flagged symbols.

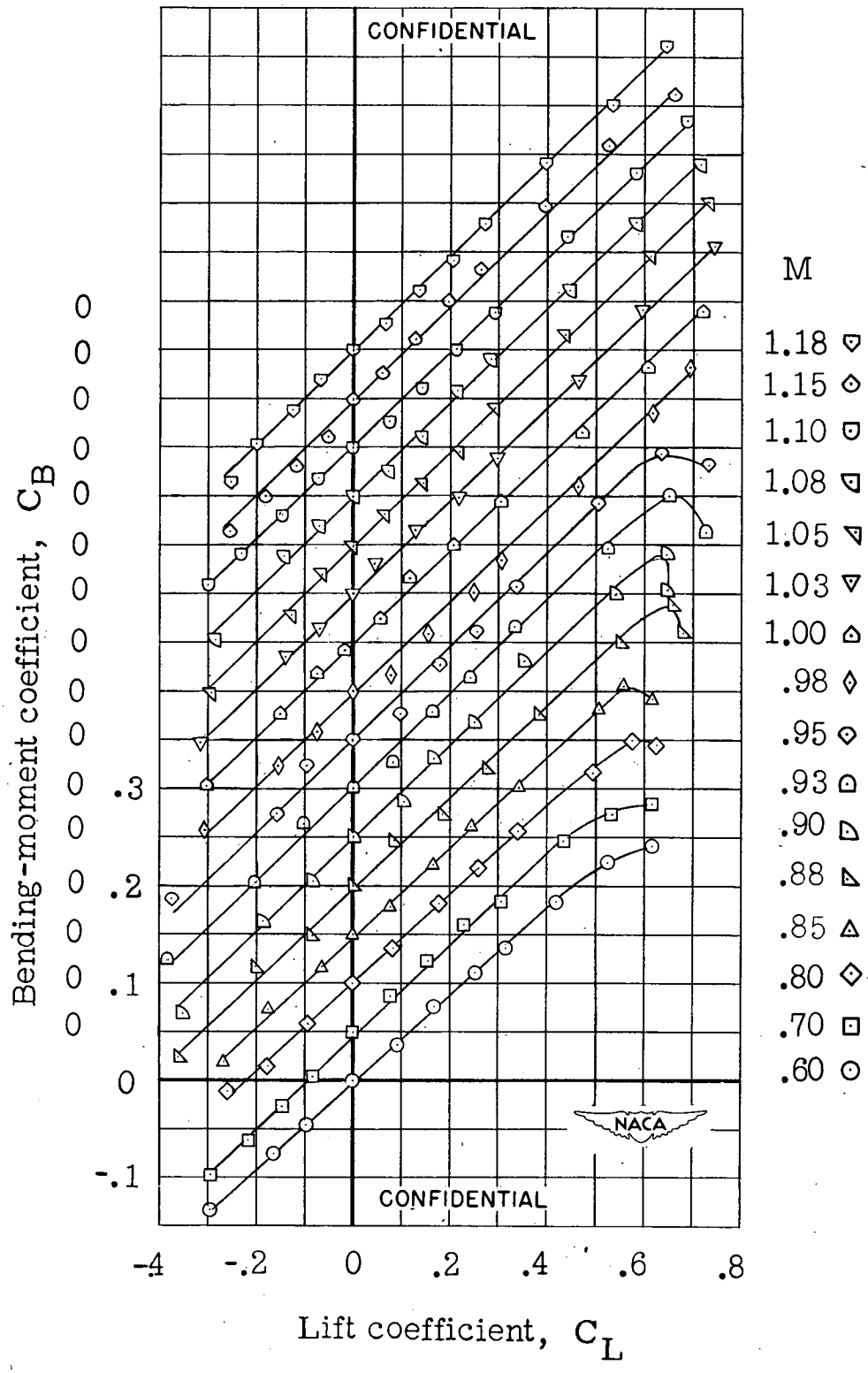

Figure 8.- Concluded.

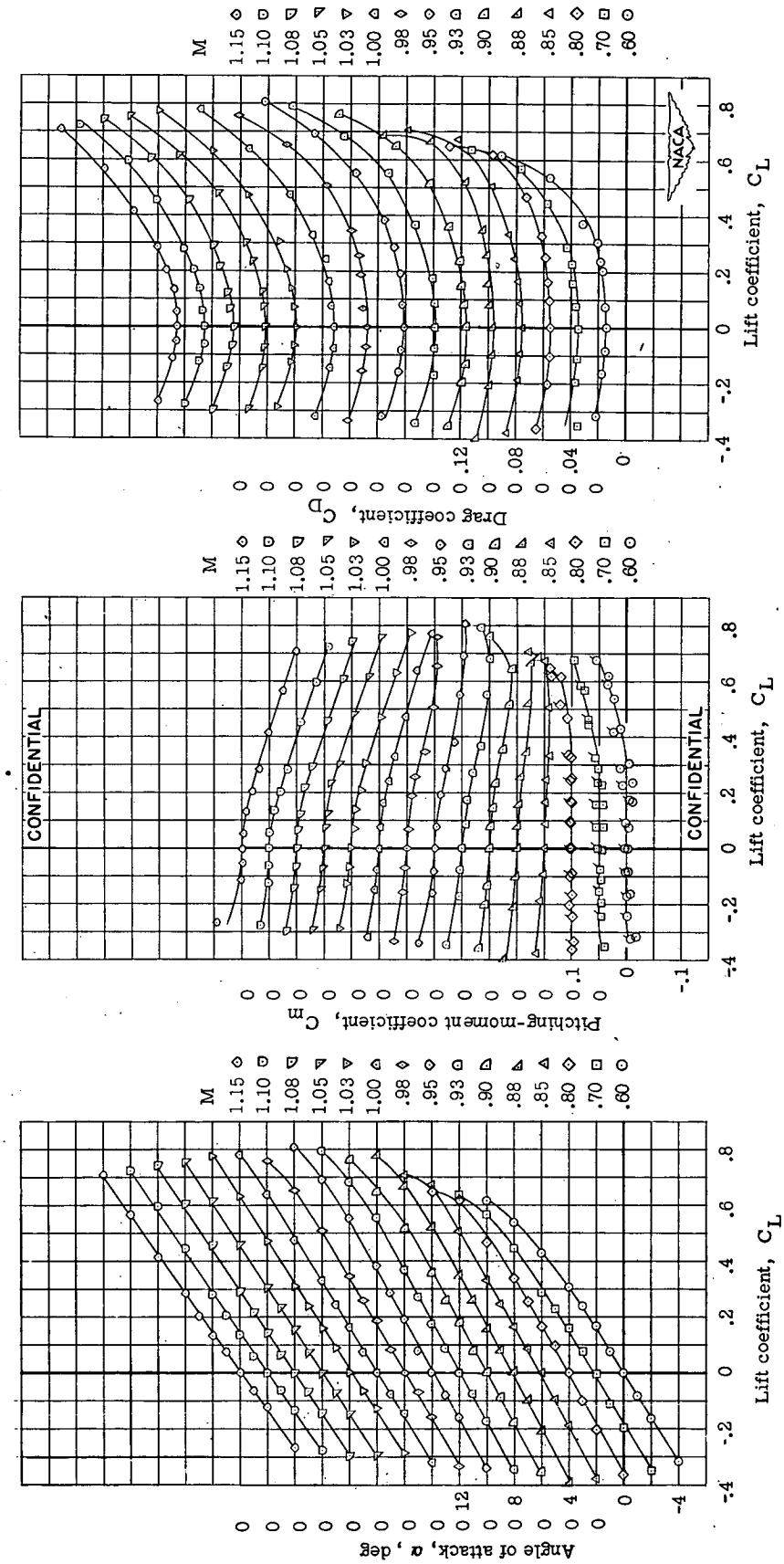

Figure 9.- Wing-fuselage aerodynamic characteristics for model with 35° sweptback wing, aspect ratio 6, taper ratio 0.6, and NACA 65A006 airfoil. Check points are indicated by flagged symbols.

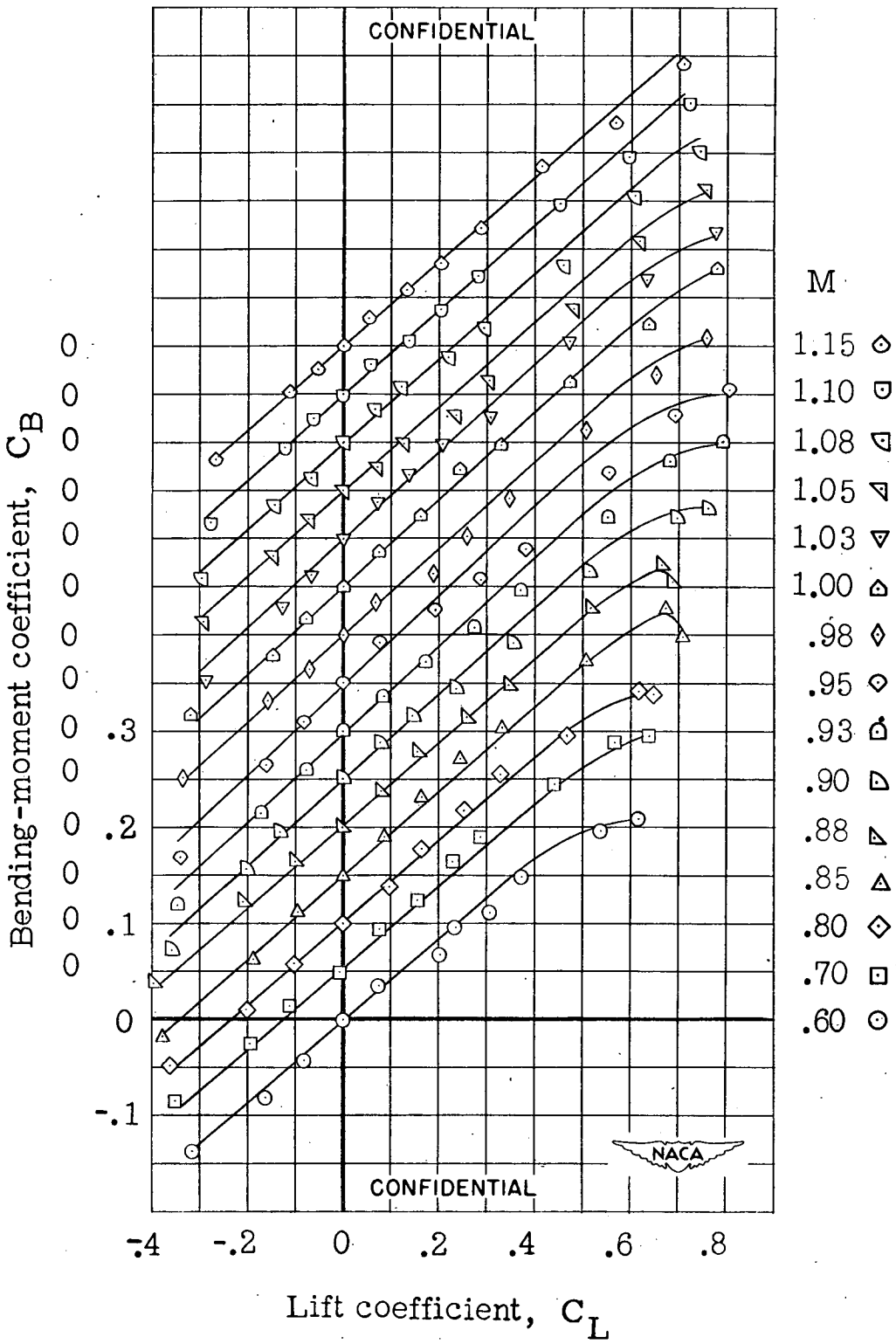

Figure 9.- Concluded.

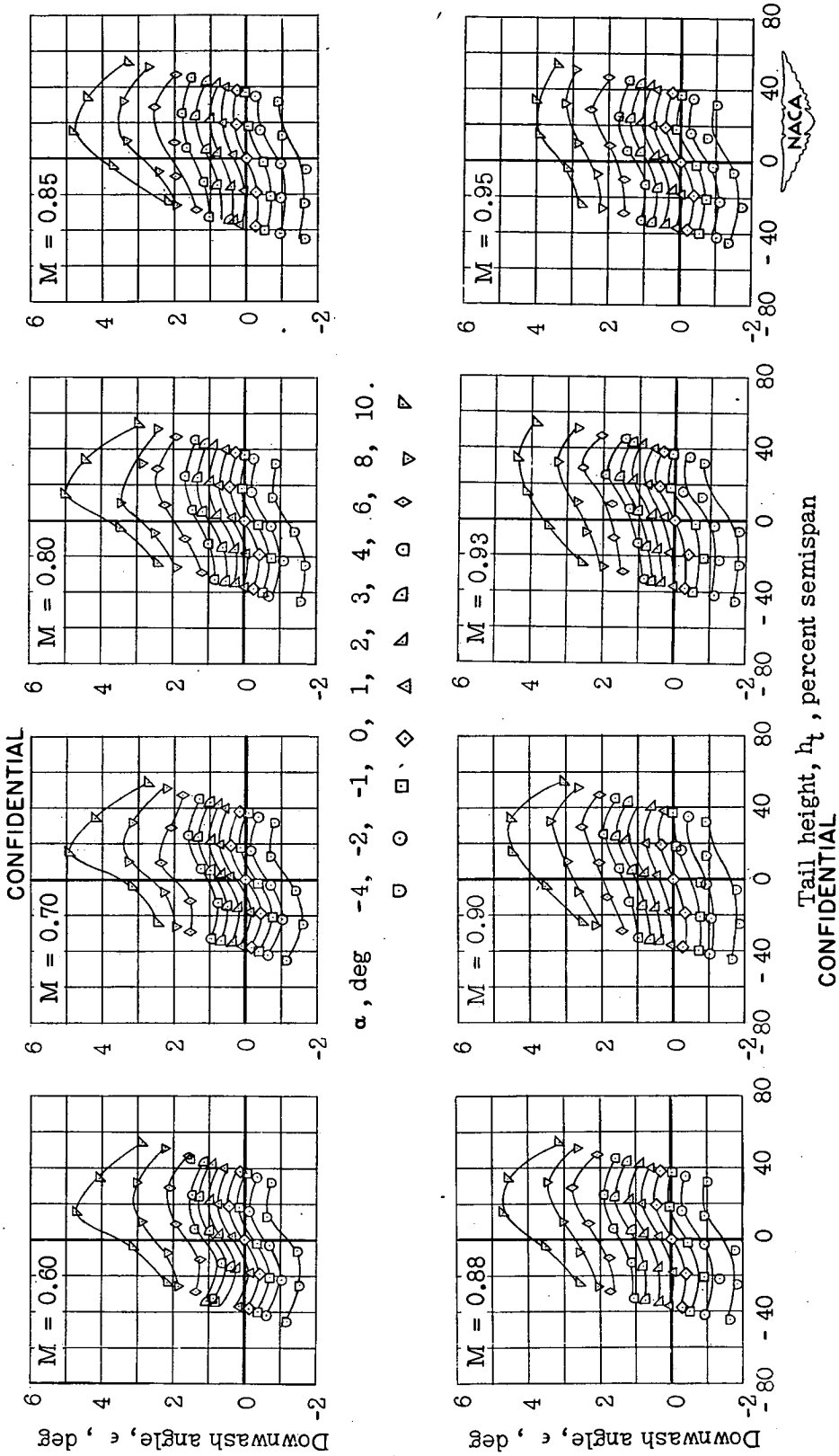

Figure 10.- Effective downwash angles in region of tail plane for model with 35° sweptback wing, aspect ratio 6, taper ratio 0.6, and NACA 65A006 airfoil. Wing alone.

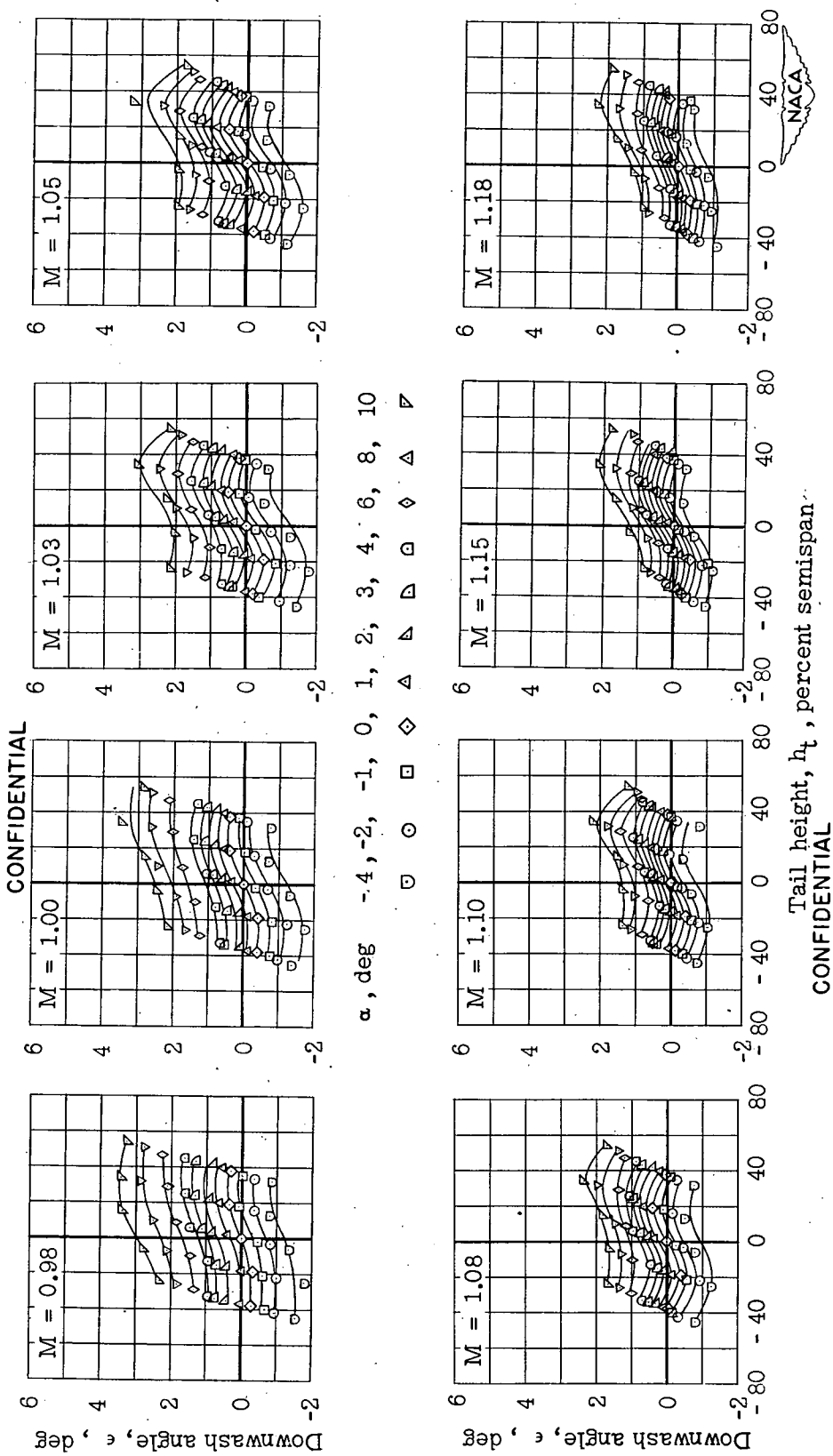

Figure 10.- Concluded.

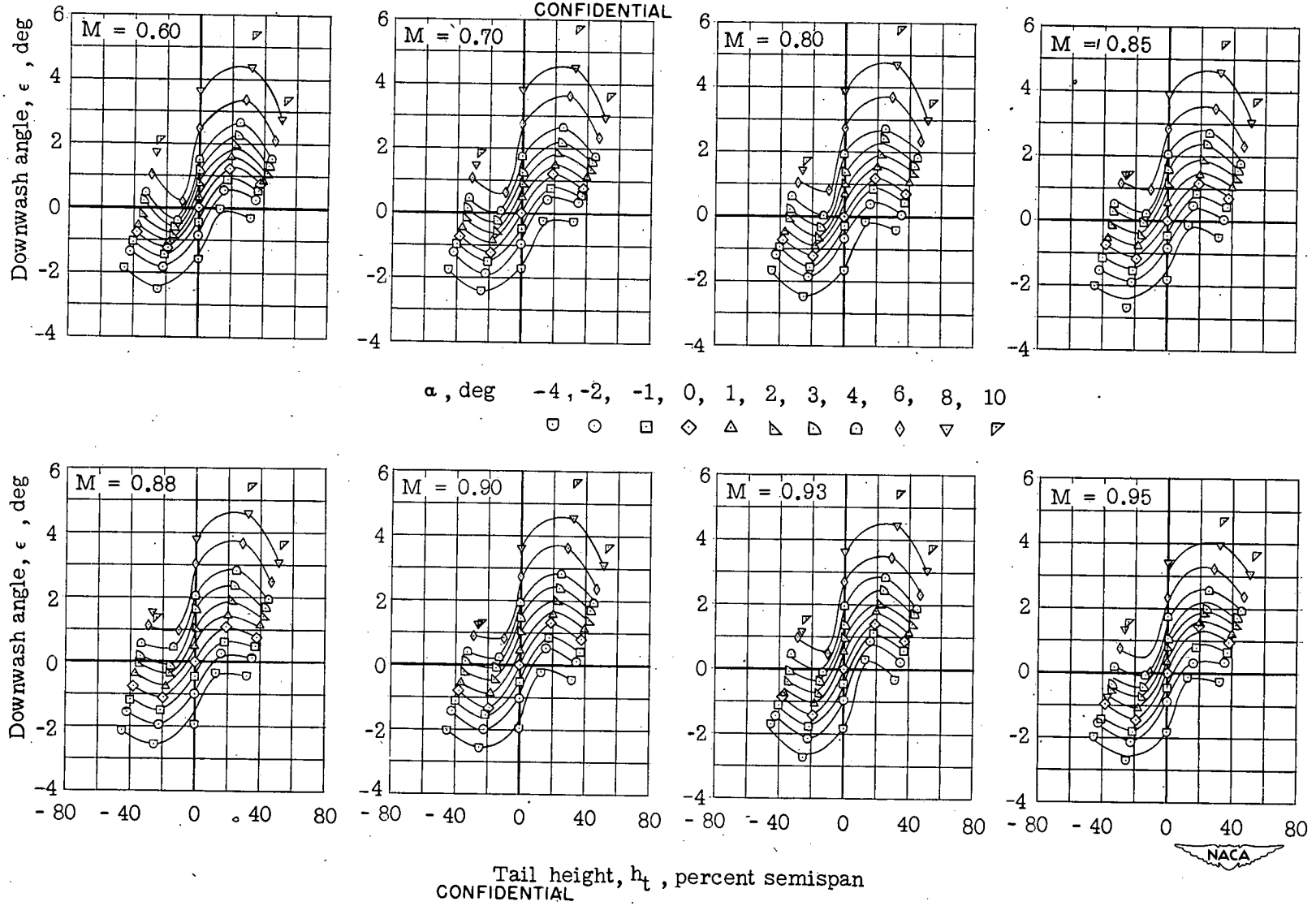

Figure 11.- Effective downwash angles in region of tail plane for model with 35° sweptback wing, aspect ratio 6, taper ratio 0.6, and NACA 65A006 airfoil. Wing-fuselage.

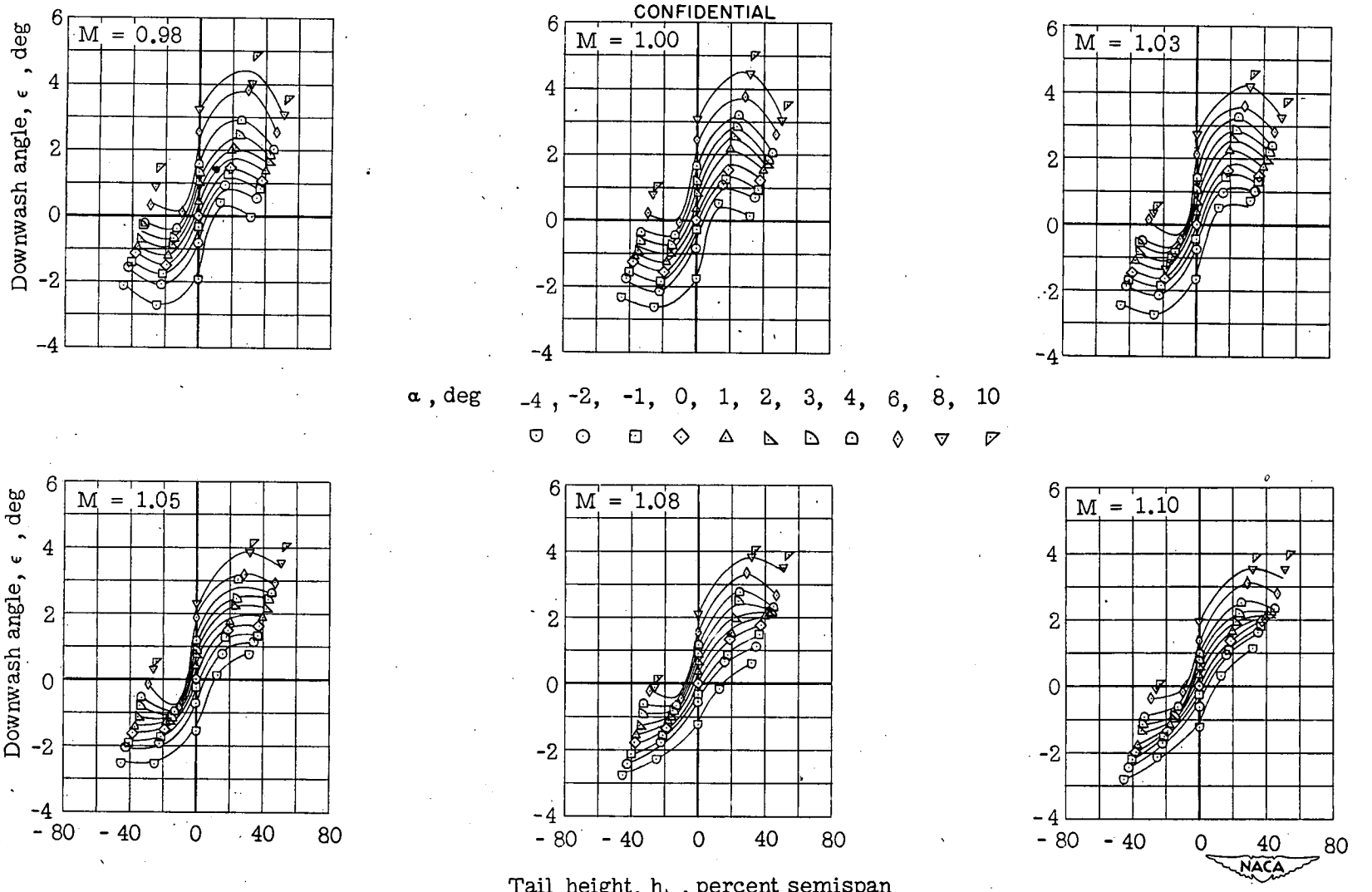

Figure 11.- Concluded.

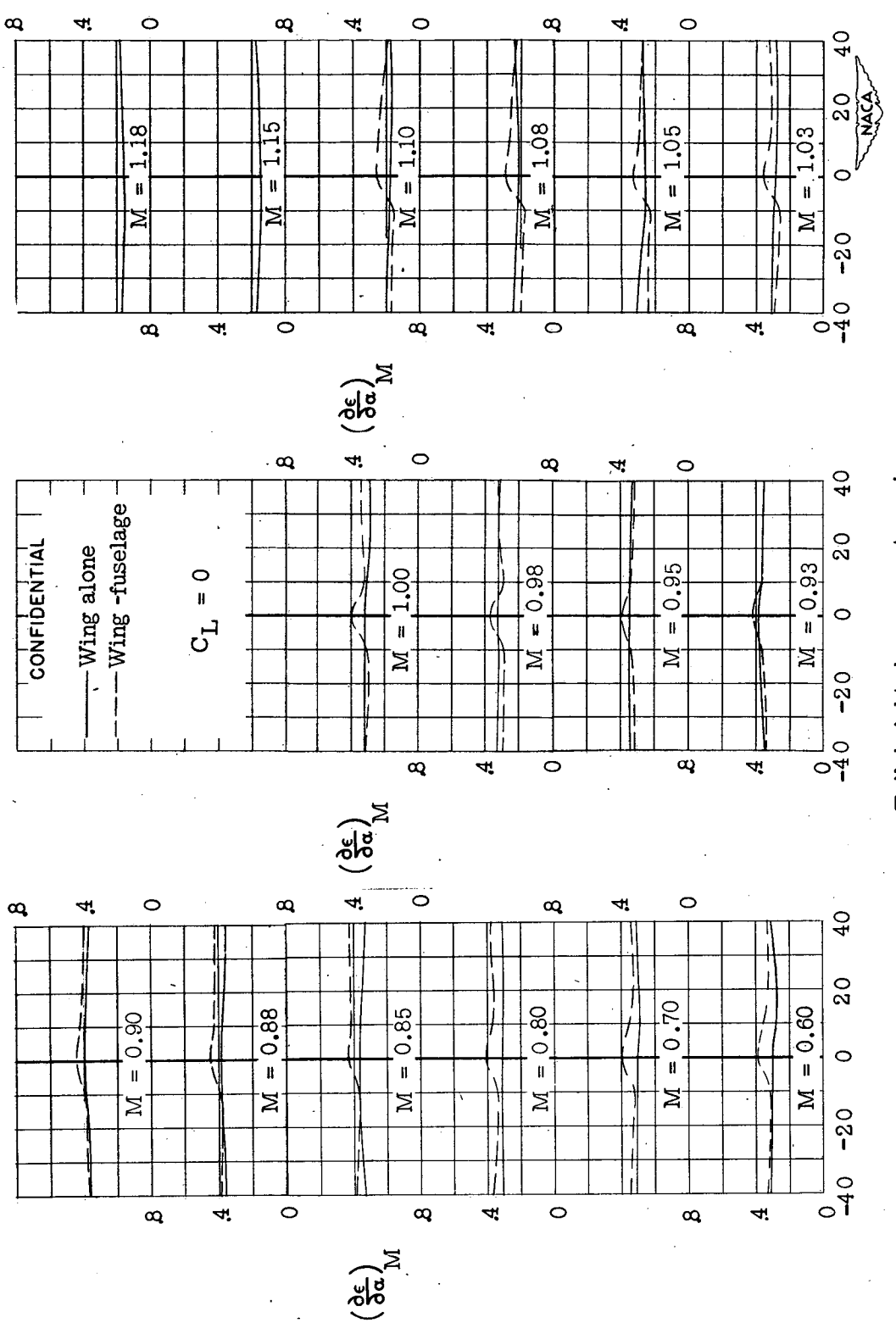

Figure 12.- Variation of downwash gradient with tail height and Mach number for model with 35° sweptback wing, aspect ratio 6, taper ratio 0.6, and NACA 65A006 airfoil.

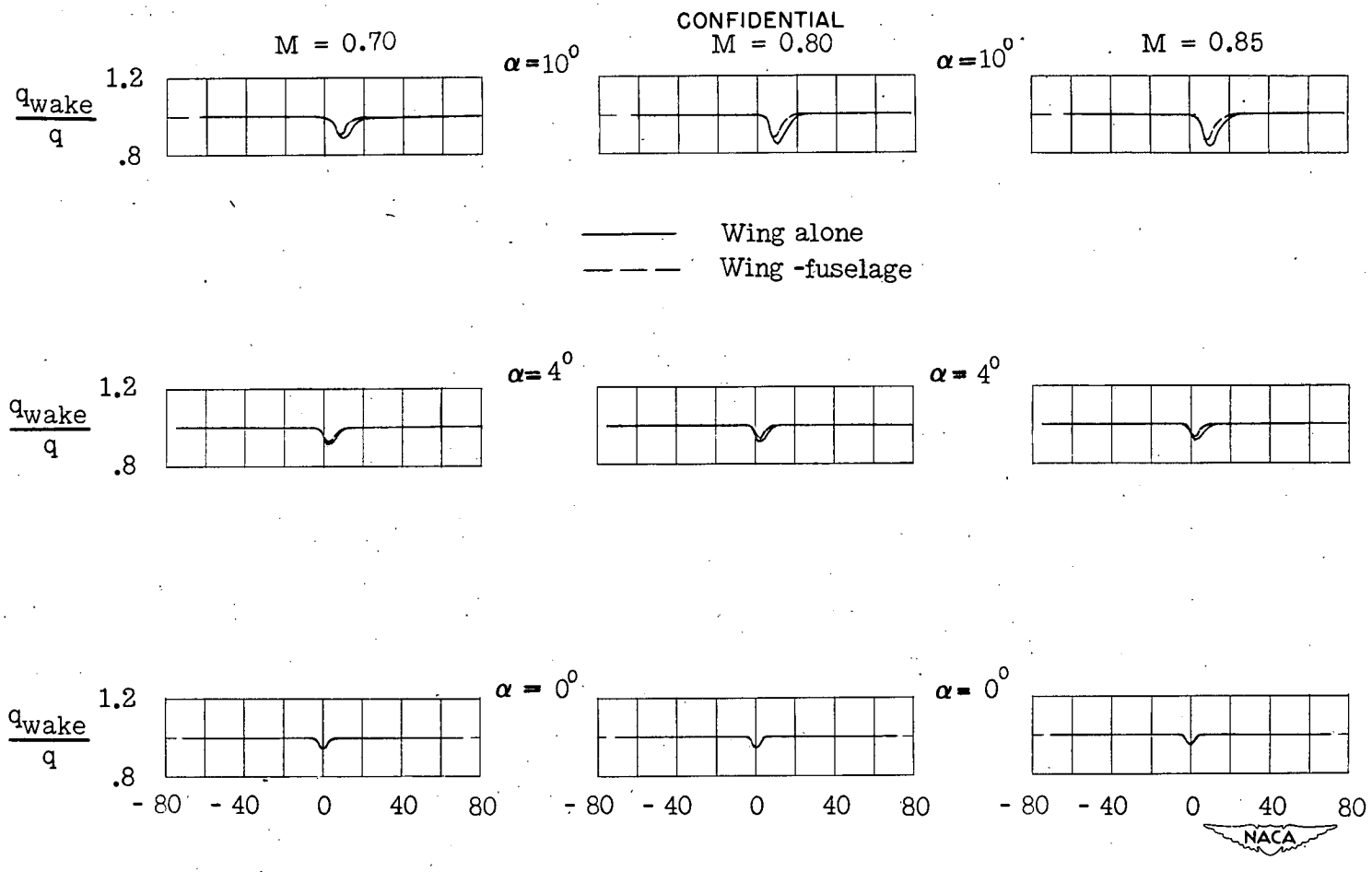

Figure 13.- Dynamic-pressure surveys in region of tail plane for model with 35° sweptback wing, aspect ratio 6, taper ratio 0.6, and NACA 65A006 airfoil.

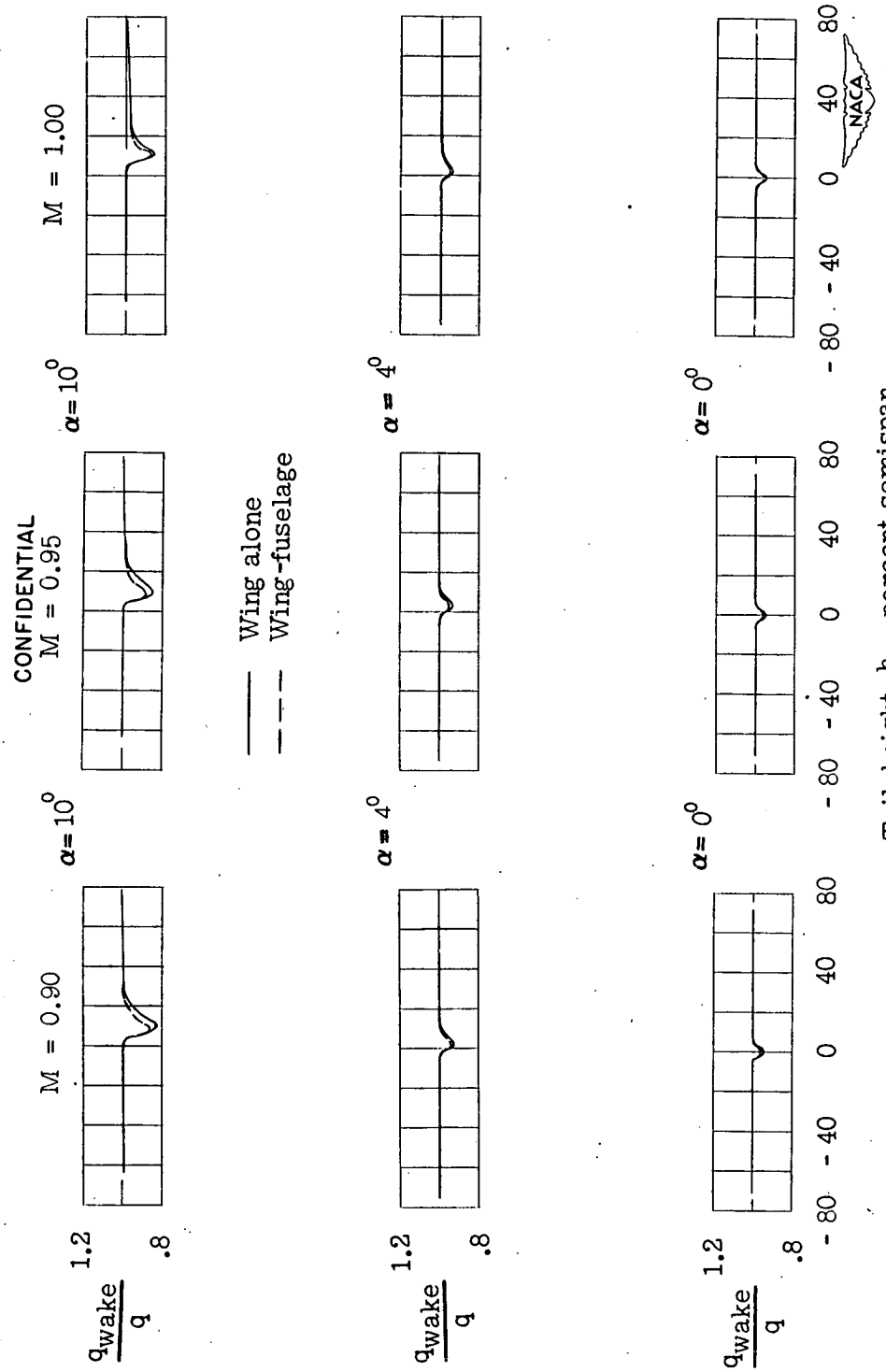

Figure 13.- Continued.

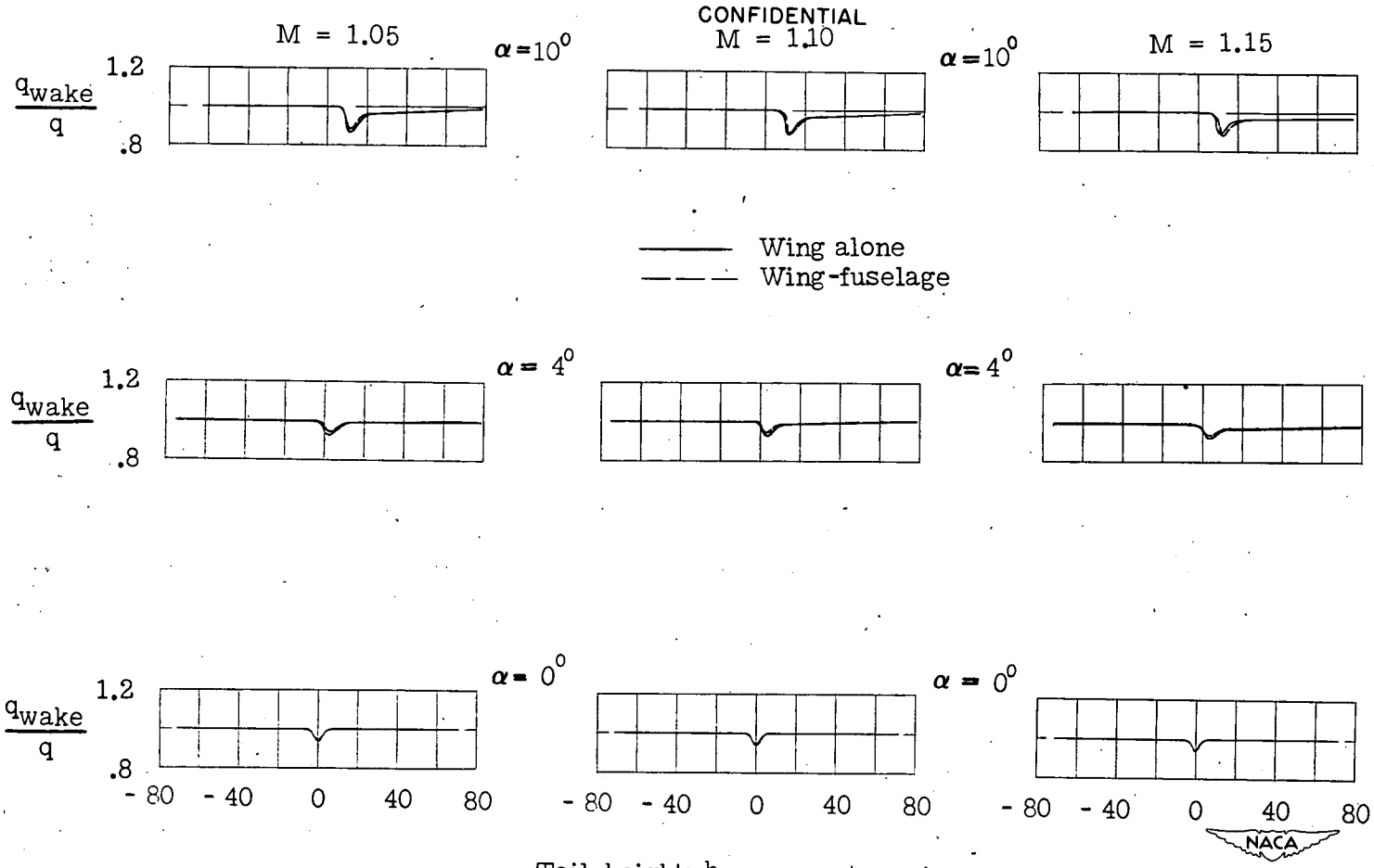

Figure 13.- Concluded.

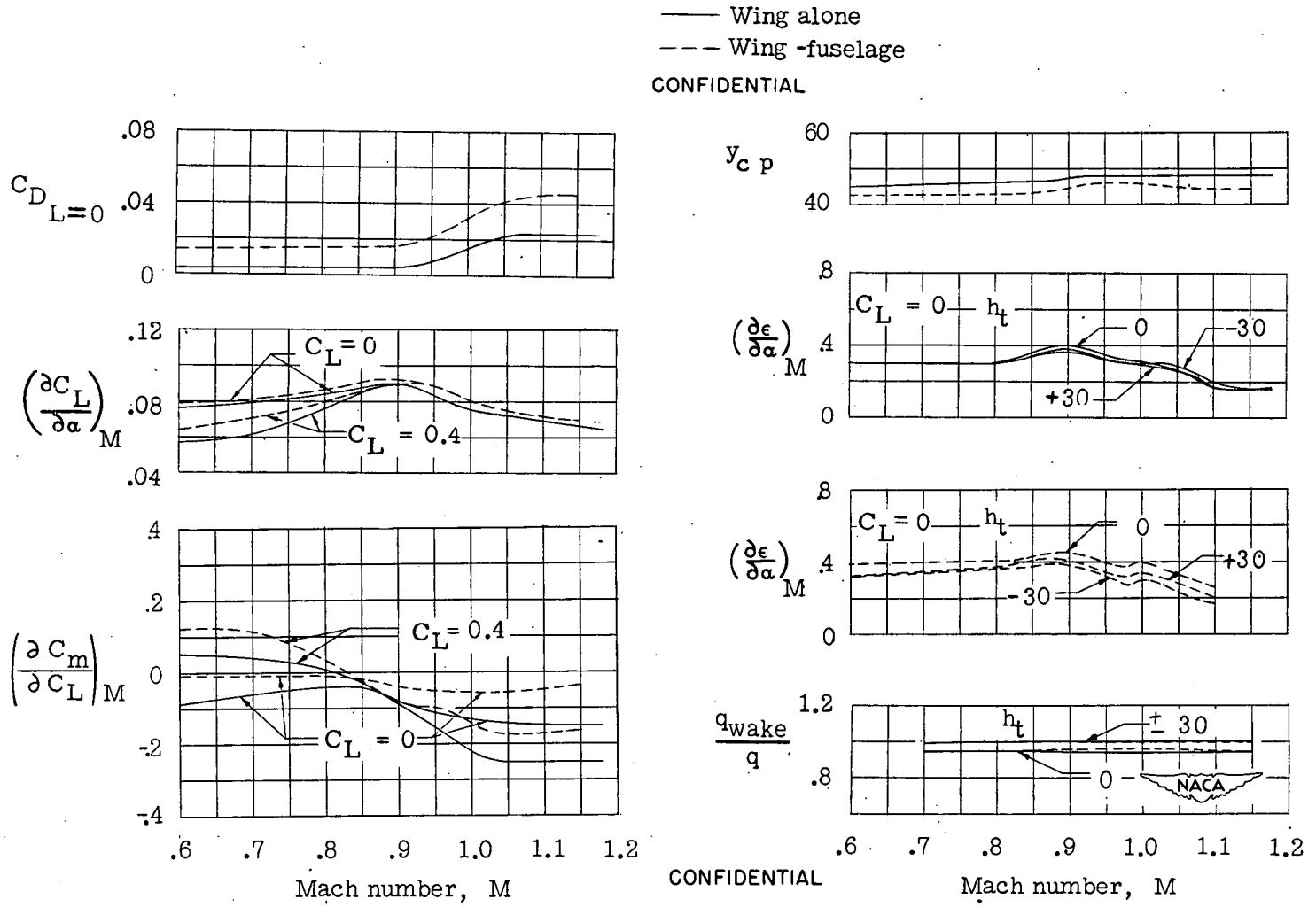

Figure 14.- Summary of aerodynamic characteristics for model with 35° sweptback wing, aspect ratio 6, taper ratio 0.6, and NACA 65A006 airfoil.

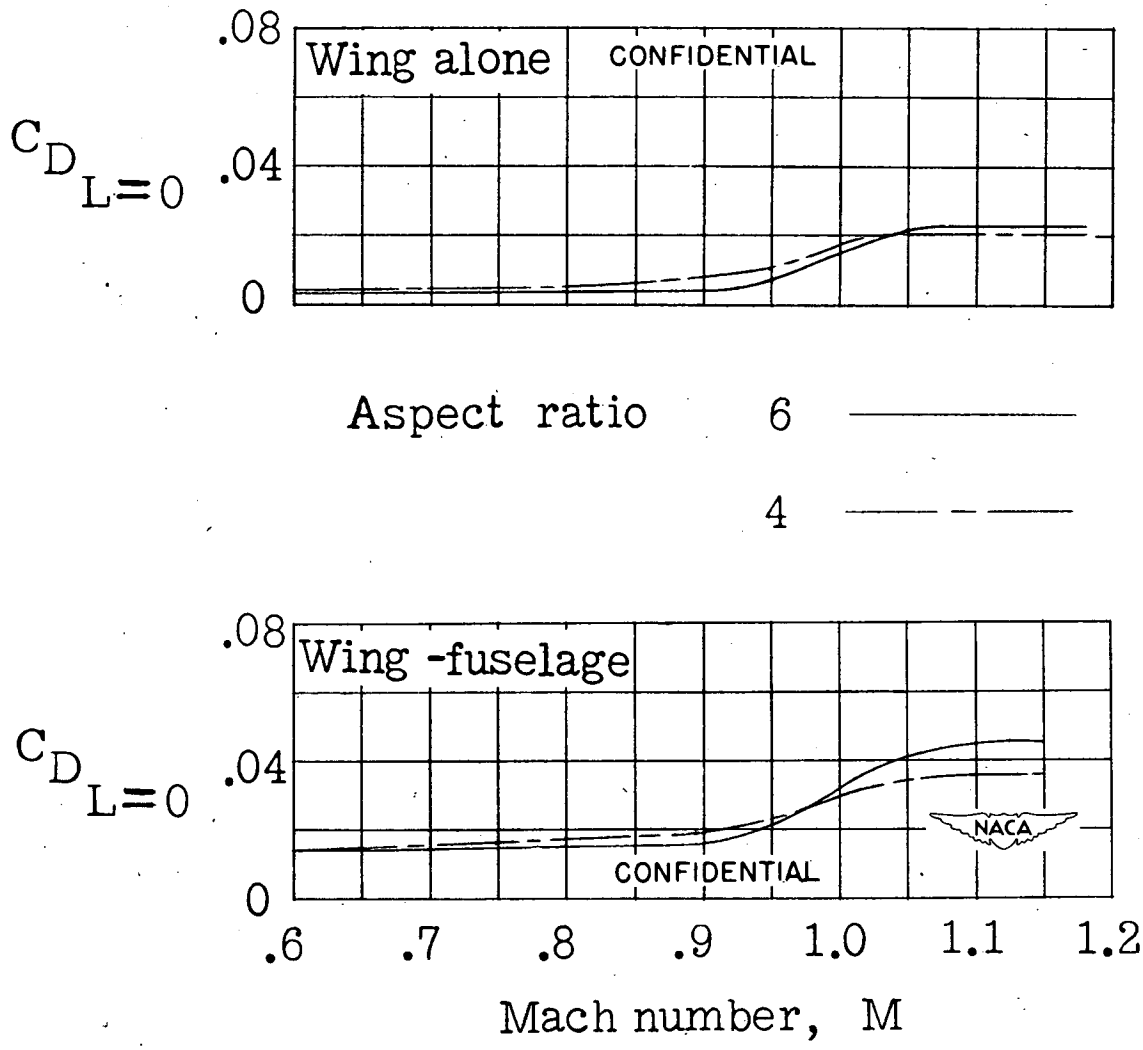

Figure 15.- Effect of aspect ratio on the minimum-drag characteristics obtained from tests using a sponge-wiper seal for wings with 35° sweepback, taper ratio 0.6, and NACA 65A006 airfoil section.